Zeng et al. Radiation Oncology (2025) 20:12
https://doi.org/10.1186/s13014-024-02568-6

Radiation Oncology

RESEARCH

Open Access

Deep learning-based synthetic CT for dosimetric monitoring of combined conventional radiotherapy and lattice boost in large lung tumors

Hongwei Zeng[1†], Xiangyu E[1†], Minghe Lv[1], Su Zeng[1], Yue Feng[1], Wenhao Shen[1], Wenhui Guan[1], Yang Zhang[1], Ruping Zhao[1*†] and Jingping Yu[2*†]

Abstract

Purpose Conventional radiotherapy (CRT) has limited local control and poses a high risk of severe toxicity in large lung tumors. This study aimed to develop an integrated treatment plan that combines CRT with lattice boost radiotherapy (LRT) and monitors its dosimetric characteristics.

Methods This study employed cone-beam computed tomography from 115 lung cancer patients to develop a U-Net + + deep learning model for generating synthetic CT (sCT). The clinical feasibility of sCT was thoroughly evaluated in terms of image clarity, Hounsfield Unit (HU) consistency, and computational accuracy. For large lung tumors, accumulated doses to the gross tumor volume (GTV) and organs at risk (OARs) during 20 fractions of CRT were precisely monitored using matrices derived from the deformable registration of sCT and planning CT (pCT). Additionally, for patients with minimal tumor shrinkage during CRT, an sCT-based adaptive LRT boost plan was introduced, with its dosimetric properties, treatment safety in high dose regions, and delivery accuracy quantitatively assessed.

Results The image quality and HU consistency of sCT improved significantly, with dose deviations ranging from 0.15% to 1.25%. These results indicated that sCT is feasible for inter-fraction dose monitoring and adaptive planning. After rigid and hybrid deformable registration of sCT and pCT, the mean distance-to-agreement was 0.80 ± 0.18 mm, and the mean Dice similarity coefficient was 0.97 ± 0.01. Monitoring dose accumulation over 20 CRT fractions showed an increase in high-dose regions of the GTV ($P < 0.05$) and a reduction in low-dose regions ($P < 0.05$). Dosimetric parameters of all OARs were significantly higher than those in the original treatment plan ($P < 0.01$). The sCT based adaptive LRT boost plan, when combined with CRT, significantly reduced the dose to OARs compared to CRT alone ($P < 0.05$). In LRT plan, high-dose regions for the GTV and $D_{95\%}$ exhibited displacements greater than 5 mm from the tumor boundary in 19 randomly scanned sCT sequences under free breathing

†First authors: Hongwei Zeng and Xiangyu E.

†Jingping Yu and Ruping Zhao have contributed equally to this work.

*Correspondence:
Ruping Zhao
fengling.36@163.com
Jingping Yu
yujingping@njmu.edu.cn

conditions. Validation of dose delivery using TLD phantom measurements showed that more than half of the dose points in the sCT based LRT plan had deviations below 2%, with a maximum deviation of 5.89%.

Conclusions The sCT generated by the U-Net + + model enhanced the accuracy of monitoring the actual accumulated dose, thereby facilitating the evaluation of therapeutic efficacy and toxicity. Additionally, the sCT-based LRT boost plan, combined with CRT, further minimized the dose delivered to OARs while ensuring safe and precise treatment delivery.

Keywords Deep learning, Synthetic CT, Dose accumulation, Lattice radiotherapy, Large lung tumor

Introduction

Conventional radiotherapy (CRT) achieves limited local control in inoperable large lung tumors, contributing to high mortality rates [1]. Stereotactic body radiation therapy (SBRT) delivers a higher biologically effective dose, improving survival outcomes in selected patients. However, studies highlight the challenges of safely administering SBRT for tumors > 5 cm due to elevated toxicity risks to surrounding organs at risk (OARs) [2–5]. Spatially fractionated radiotherapy (SFRT) facilitates safe dose escalation in large lung tumor treatment [6]. Initially, SFRT used custom collimators to create 2D treatment plans resembling GRID radiotherapy, producing high-dose peaks in tumors. Although effective for large superficial tumors, SFRT is limited in treating deep-seated tumors (> 8 cm from the surface), as it risks excessive radiation to adjacent healthy tissues [7–10].

Lattice radiotherapy (LRT) overcomes these limitations by transforming 2D GRID principles into a 3D configuration, establishing high-dose regions at defined intervals within the tumor. The vertice-valley dose distribution reduces OARs exposure. However, clinical experience with LRT is limited, and its biological mechanisms remain under investigation [11–13]. Furthermore, standardized dosimetric guidelines for LRT, including high-dose region distribution and dose-volume histogram (DVH) parameters, are not yet established. Consequently, CRT, delivering 60–66 Gy, remains the standard for treating large lung tumors [14, 15]. Clinically, LRT is often combined with CRT to enhance efficacy, with CRT delivering a uniform dose that augments valley dose effects. Palliative LRT is typically applied before, after, or interspersed with CRT [16]. The Scandinavian NARLAL2 Phase III trial (NCT02354274) underscores the need to monitor OARs toxicity during dose escalation [17]. Dynamic tumor volume changes during treatment may lead to discrepancies between simulated and actual doses to normal tissues, complicating cumulative dose estimation in LRT boost protocols [18–20].

Advances in image-guided radiotherapy (IGRT) and adaptive radiotherapy (ART) offer promising solutions. Daily cone-beam computed tomography (CBCT) provides high-resolution imaging for continuous anatomical monitoring during treatment [21–23]. Additionally, deep learning algorithms improve organ segmentation accuracy, suppress artifacts, and generate high-quality synthetic CT (sCT) images for dose calculation. Collectively, these technologies enable more precise dose monitoring, enhancing the feasibility of combining conventional and Lattice radiotherapy [24–26].

This study proposed a clinical protocol to monitor the dosimetric performance of combined CRT and LRT boost plans for large lung tumors. The protocol administered 40 Gy of CRT to the entire tumor over 20 fractions. Retrospective analysis using sCT generated by deep learning model assessed the cumulative dose to the tumor and OARs. For patients with less than a 5% reduction in tumor volume after 20 fractions, and tumor volumes exceeding 200 cm^3, an adaptive LRT boost plan was formulated using sCT. Dose evaluation clarified toxicity to OARs, and dosimetric quality control ensured precise beam delivery for the adaptive LRT boost.

Methods

Data collection

This study retrospectively analyzed 115 primary lung cancer patients who underwent radiotherapy from December 2022 to February 2024. Patient ages ranged from 63 to 88 years, with a median age of 76 years (SD = 7). Planning CT (pCT) scans were acquired using a SOMATOM Confidence 20 CT scanner (Siemens, BER, GER) at 120 kV with a slice thickness of 5 mm. Daily CBCT images were obtained with the Halcyon linear accelerator (Varian, CA, USA), employing a thoracic protocol of 125 kV, 294 mAs, and a slice thickness of 2 mm.

U-Net + + based CBCT to sCT generation

The U-Net + + deep learning model network architecture was illustrated in Fig. 1. For model training, paired pCT and initial CBCT images were acquired from 85 lung cancer patients, with 30 patients allocated for validation. Both imaging modalities underwent preprocessing to reduce non-anatomical artifacts. Rigid registration aligned the pCT and CBCT

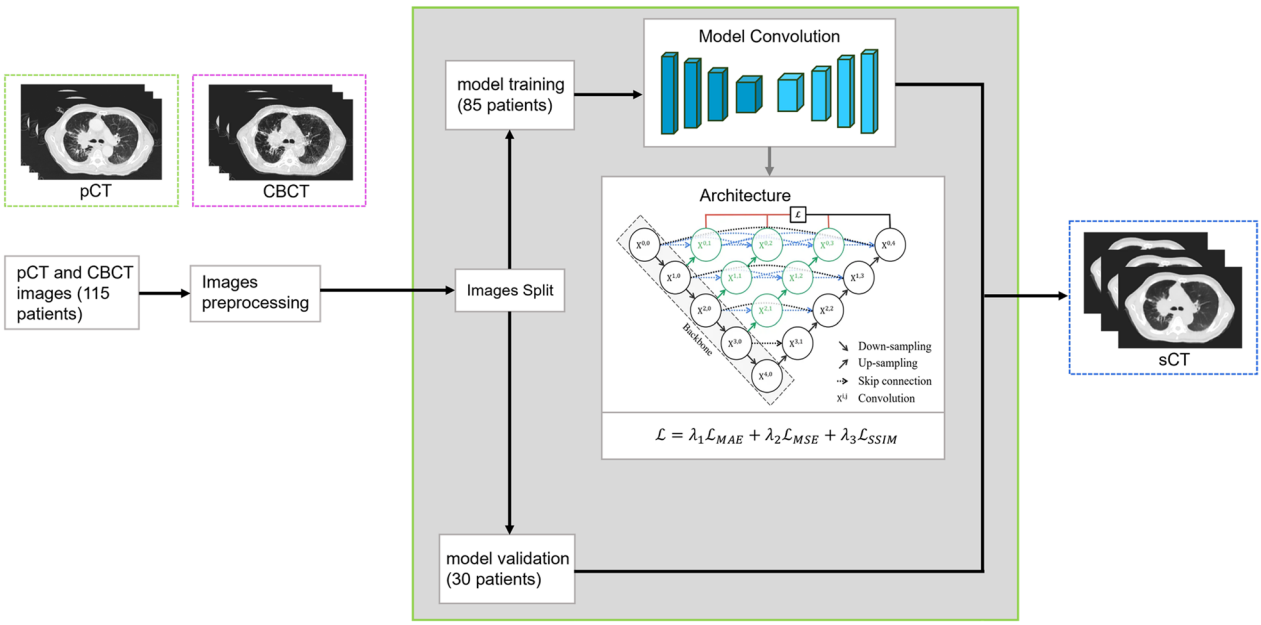

Fig. 1 Network architecture of U-Net + + deep learning model

images, which were then cropped to a standardized size of 512 × 512 pixels and a slice thickness of 3 mm. Automatic thresholding differentiated between internal and external body regions, excluding external voxels from dose calculations by assigning a value of − 1000 Hounsfield Units (HU). Z-score normalization standardized the intensity range from − 1000 to 3000 HU. The model employed an encoder-decoder framework. The encoder, based on ResNet50, extracted five feature representations, denoted as $x^{i,0}$, across various scales, focusing on feature extraction. The model utilized a composite loss function ($\mathcal{L}$) that integrates three components: mean absolute error (MAE), mean squared error (MSE), and structural similarity index measure (SSIM) loss [27]. The contributions of these components were adjusted using hyperparameters λ_1, λ_2 and λ_3, established through iterative experimentation and cross-validation.

Calculations for the MAE and MSE losses were limited to the body region. Due to the significant differences between CBCT and pCT, the SSIM was employed to optimize output brightness, contrast, and structural fidelity. All experiments were conducted using PyTorch version 1.10.1 on an RTX A6000 GPU (NVIDIA, CA, USA). To enhance model robustness during training, random data augmentation was applied with a probability of 0.5, utilizing techniques such as rotation, translation, and mirroring. Training was conducted using the Adam optimizer, initialized with a learning rate of $1e^{-4}$ and a batch size of 16. The training process spanned a total of 200 epochs, with each epoch requiring approximately 90 min.

sCT based dose calculation accuracy evaluation

To evaluate the model's dose calculation accuracy, paired pCT and CBCT images were obtained from 30 lung cancer patients within a 24 h interval. The sCT images were generated using a U-Net + + model. Automatic contouring of OARs, including Lungs, heart, and spinal cord, was performed on both pCT and sCT using the RT-Mind auto-contouring system (Medmind, BJ, CN). The gross tumor volume (GTV) was manually contoured by an experienced radiation oncologist. Structures on the CBCT were derived from the sCT and underwent a comprehensive review and refinement process. Treatment plans for both intensity modulated radiation therapy (IMRT) and volumetric modulated arc therapy (VMAT) were developed on the sCT, yielding a total of 60 cases. IMRT was planned using 9 fields at 40° intervals, while VMAT employed dual full arcs. Dose calculations for both treatment plans were performed using the Acuros XB algorithm. Following rigid registration of the sCT with both the pCT and CBCT, the dose maps were transferred to the pCT and CBCT for dose calculation accuracy evaluation of the GTV and OARs.

Inter-fraction dose accumulation

This phase involved 13 patients with large lung tumors whose GTV exceeded 200 cm^3 after 20 sessions of CRT, showing a GTV volume reduction of less than 5%. The

sCTs were generated from CBCT obtained during the 5th, 10th, 15th, and 20th treatment fractions, adhering to a standardized thoracic scanning protocol. The dose accumulation process across the radiation therapy fractions was structured into three distinct steps as shown in Fig. 2.

In the first step, a hybrid intensity deformation registration algorithm was employed with RayStation v9.0 (RaySearch Laboratories AB, Stockholm, Sweden), designating the pCT as the target image and the sCT as the source image for the deformable registration process. Before this registration, both the pCT and sCT underwent rigid registration to correct global misalignments, including translation, rotation, and scaling, thereby ensuring precise alignment of anatomical structures. The clinical regions of interest (ROIs) on the pCT, including GTV, lungs, and heart, were compared with those mapped from the sCT to the pCT through deformable registration, employing mean distance-to-agreement (DTA) and mean Dice similarity coefficient (DSC) for the quantitative validation of both rigid and deformable registration.

In the second step, the deformation matrix obtained from the deformable registration was applied to the dose distribution maps from the four sCTs, resulting in deformed dose distributions. This process accounted for patient-specific anatomical changes across treatment sessions, allowing for accurate mapping of dose distributions from sCT to pCT. B-spline and diffeomorphic transformation algorithms ensured smooth and anatomically consistent dose warping, correcting discrepancies in organ shape and position throughout the treatment course.

Finally, the deformed dose distributions from the four sCT fractions were accumulated onto pCT. A dosimetric analysis compared the accumulated dose to the initial treatment plan, primarily focusing on the GTV and OARs. Key parameters, including target coverage and dose-volume metrics for normal tissues, were evaluated to ensure that the accumulated dose remained within clinically acceptable limits.

sCT based adaptive LRT boost plan

Currently, clinical data on dosimetric guidelines for LRT are insufficient. In the previous phase, 13 patients with large lung tumors, who demonstrated inadequate tumor regression after 20 sessions of CRT, were identified as suitable candidates for clinical scenarios requiring LRT. This study devised an adaptive LRT boost plan that utilized sCT generated from the twentieth fraction of CBCT acquired post-CRT. The treatment prescription was predicated on delivering a total dose of 20 Gy in two fractions to the high-dose vertices using 6 MV photons, in accordance with the typical geometric and dosimetric parameters illustrated in Fig. 3 [28].

The layout of the vertices was initially established without stringent requirements regarding the symmetry of vertex placement or the uniformity of their size and shape. The total number of vertices was contingent upon the size and shape of the tumor volume. The adaptive

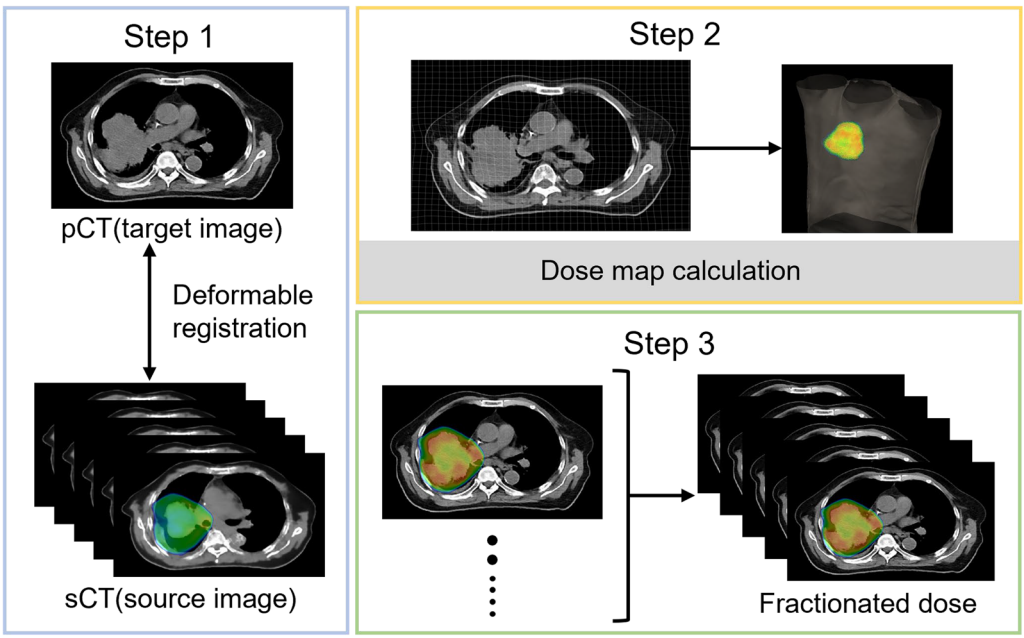

Fig. 2 Workflow of dose accumulation

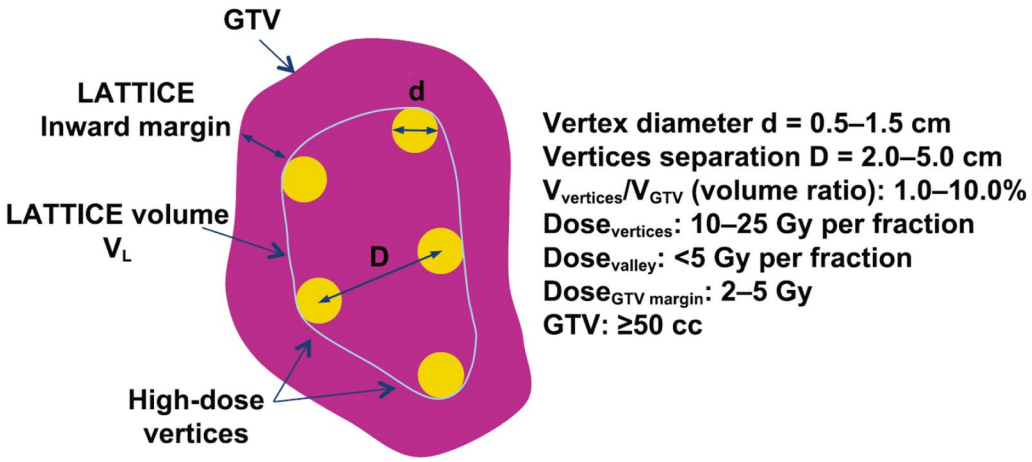

Fig. 3 Parameters and ranges of a typical LRT plan

LRT boost plan developed in this study employed geometrically arranged spherical vertices, with the quantity set to 6–8 based on the GTV, each possessing a diameter of 15 mm and spaced 20–50 mm apart, while maintaining a volume ratio of the vertices to the GTV between 3 and 4%. In light of the challenges associated with managing respiratory motion in patients with large lung tumors, vertices situated more than 10 mm within the GTV margins were excluded to ensure a safe distance from the tumor boundary, thereby minimizing the risk of dose spill beyond the target for the 20 Gy treatment. VMAT was utilized to generate a high-dose gradient within the tumor target region. Compared to IMRT and 3D conformal radiation therapy, VMAT offered superior target coverage while minimizing high-dose leakage and exposure to OARs. The LRT plan prescription delineated both the vertices dose and the valley dose. The vertices dose was established to encompass 95% of the prescribed dose. To induce anti-tumor immunity, the valley dose was required to be less than 5 Gy (or as low as reasonably achievable). However, for patients undergoing palliative treatment, the specific value of the valley dose was not strictly defined. The adaptive LRT boost plan was executed using the Halcyon linear accelerator platform and the Eclipse v16.1 (Varian, CA, USA) treatment planning system (TPS), featuring a minimum multileaf collimator resolution of 5 mm. Plans were optimized with the biological target generalized equivalent uniform dose (EUD) method without controlling for hotspots within the lattice structures. The implementation of VMAT enabled continuous radiation delivery during arc rotation, allowing precise modulation of dose distribution and enhancing conformity to the tumor shape.

To further evaluate the off-target risk associated with the adaptive LRT boost plan in the treatment of patients with large lung tumors, this study utilized sCT generated from CBCT scans of the 13 patients after their initial 19 sessions of CRT. The adaptive LRT boost plan was rigidly registered using GTV as ROI with the 19 sets of images, facilitating the delineation and transplantation of vertices and structure generated by 95% prescription dose ($D_{95\%}$) onto the sCT for the purpose of assessing the shortest relative displacement of the vertices from the GTV boundary. The consistent stability of tumor volume in these patients throughout the course of CRT established a foundation for the assessment.

During the treatment delivery phase, thermoluminescent dosimeter (TLD) measured the dose distribution of the LRT plan within a heterogeneous anthropomorphic phantom (702 D, CIRS, Norfolk). A total of 20 measurement points were selected for dose assessment, including 16 vertice points and 4 valley points. Repeat the measurement 3 times to reduce systematic error. The TLD detectors were calibrated under simulated irradiation conditions at the National Institute of Metrology in China, utilizing 6 MV FFF photons at doses of 0.1, 1, and 2 Gy. The calibration experiments demonstrated a significant linear relationship between the doses and the TLD responses across various ranges.

Statistics analysis

Statistical analyses were performed using Python v3.9.16, with data presented as mean ± standard deviation $\overline{x} \pm s$. The Shapiro–Wilk (S–W) test assessed normality. Paired sample t-tests were conducted for datasets meeting the normality assumption, while non-parametric tests were used for those that did not. A P-value of < 0.05 was deemed statistically significant.

Results

Figure 4 provides a visual comparison of CBCT, pCT, and sCT, demonstrating that sCT significantly enhances image quality compared to CBCT and closely resembles the reference pCT. The sCT effectively reduced scatter artifacts while preserving anatomical fidelity and enhancing clarity attissue boundaries.

To further illustrate the synthesis effects of the U-Net + + model, differences were calculated by subtracting both CBCT and sCT from pCT, as shown in Fig. 4. Darker colors indicated larger differences, with darker shades representing greater variability. The overall difference between the sCT and pCT was significantly smaller than the difference observed in CBCT, especially in regions characterized by tumors and extensive soft tissue. Conversely, the model exhibited comparatively less effective control over HU values at the interfaces of bony structures.

Figure 5 presents the dose calculation accuracy derived from sCT. The short interval for acquiring pCT and CBCT was designed to ensure anatomical consistency and minimize calculation errors. In the 60 cases involving IMRT and VMAT verification plans, the differences in dosimetric parameters ($D_{2\%}$, $D_{50\%}$, and $D_{98\%}$) for the GTV were below 1%. For the OARs, three of six dosimetric parameters were below 1%, with the maximum difference in D_{mean} for the heart being 1.25%.

The cumulative dose between fractions is derived from the deformation matrix. In this study, the registration protocol comprised rigid registration followed by deformable registration. Table 1 details the quantitative improvements in spatial accuracy across the three sites. Comparing the mean values ± standard deviation of rigid registration and those obtained from deformable registration revealed that the mean DTA improved from 8.21 ± 4.72 mm to 0.80 ± 0.18 mm (amelioration of 87.66%), and the mean DSC improved from 0.60 ± 0.08 to 0.97 ± 0.01 (amelioration of 63.10%).

Leveraging the acceptable accuracy of sCT dose calculations and deformation matrices, we recalculated the doses based on the original plan for the 5th, 10th, 15th, and 20th sCT fractions. The dose distributions for these four fractions were subsequently transferred to the pCT using the deformation matrix for dose accumulation. A comparative analysis of the accumulated dose distribution and the original plan in the OARs is presented in Fig. 6. The $D_{98\%}$ value within the GTV increased ($P < 0.05$), while the $D_{2\%}$ value decreased ($P < 0.05$), indicating reduced uniformity in the actual radiation dose delivered to the tumor and diminished prescription dose coverage. Additionally, the dosimetric performance analysis of the OARs showed that all parameters exhibited varying degrees of accumulated dose increase compared to the original plan ($P < 0.01$). These deviations significantly compromised treatment precision and increased the risk of cardiopulmonary toxicity.

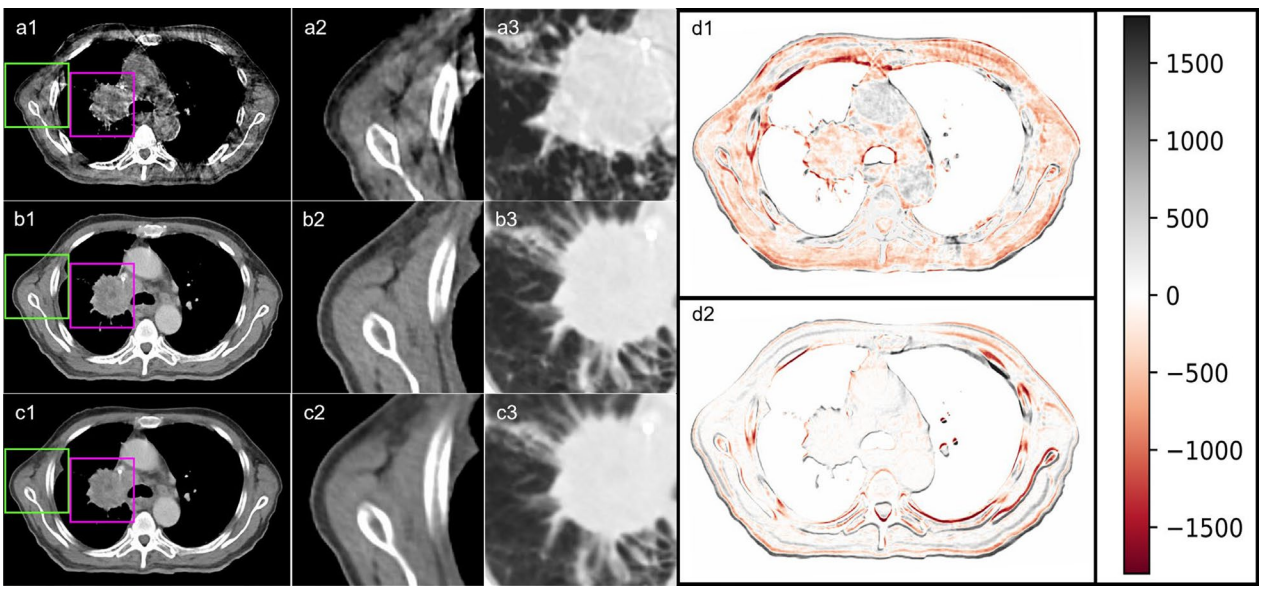

Fig. 4 Comparison of different images: Panel **a1**, **b1**, and **c1** represented a slice of CBCT, pCT, and sCT, respectively; panel **a2**, **b2**, and **c2** showed soft tissue and bony structure comparisons in the green boxed region under the soft tissue window; panel **a3**, **b3**, and **c3** showed tumor tissue comparisons in the pink boxed region under the lung window; panel **d1** showed the HU value differences between CBCT and pCT, while panel **d2** showed the HU value differences between sCT and pCT

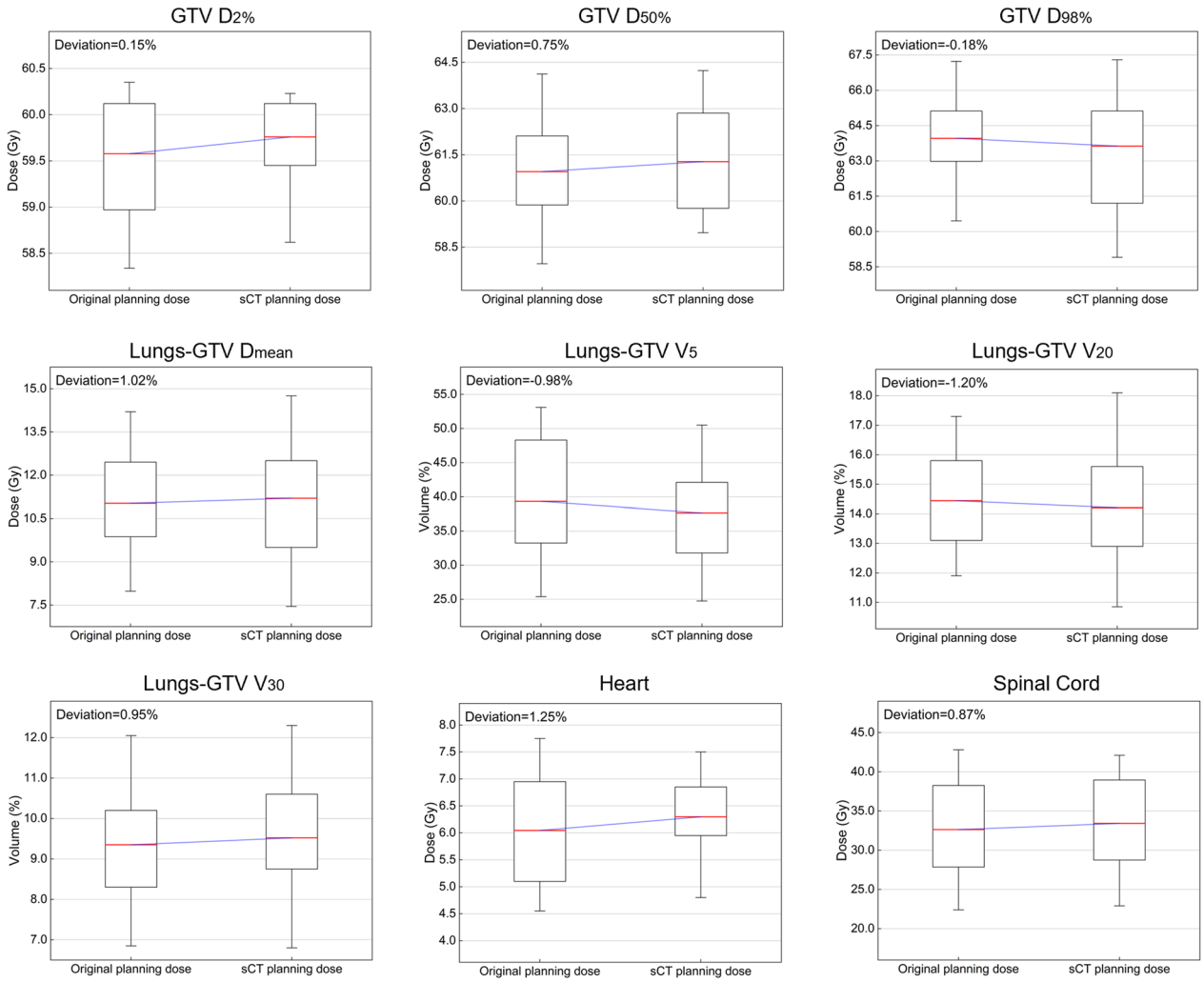

Fig. 5 Comparison of doses between the original plans and the sCT based plans (n = 60)

Table 1 Image registration results across three clinical ROIs

ROIs	Mean DTA (mm)			Mean DSC		
	Rigid registration	Deformable registration	Amelioration (%)	Rigid registration	Deformable registration	Amelioration (%)
GTV	1.47 ± 1.38	0.28 ± 0.07	80.95	0.63 ± 0.10	0.98 ± 0.01	55.56
Lungs	12.56 ± 7.42	1.32 ± 0.25	89.49	0.55 ± 0.08	0.97 ± 0.01	76.36
Heart	10.61 ± 5.37	0.79 ± 0.21	92.55	0.61 ± 0.07	0.96 ± 0.01	57.38

The sCT based adaptive LRT boost plan represents an innovative approach in clinical practice. As illustrated in Fig. 7, its dose distribution aligned with classic LRT characteristics while significantly diverged from those of CRT. Although the maximum dose was comparable to that of CRT, the distribution area and volume differed. Notably, low doses (5 Gy) markedly reduced scattering to normal tissues, especially in the affected lung and cardiac regions. This effective control of scattering can further mitigate radiotherapy toxicity in patients with large lung tumors.

Table 2 quantitatively illustrates the optimization of radiation doses to various OARs when the adaptive LRT boost plan was combined with CRT, compared

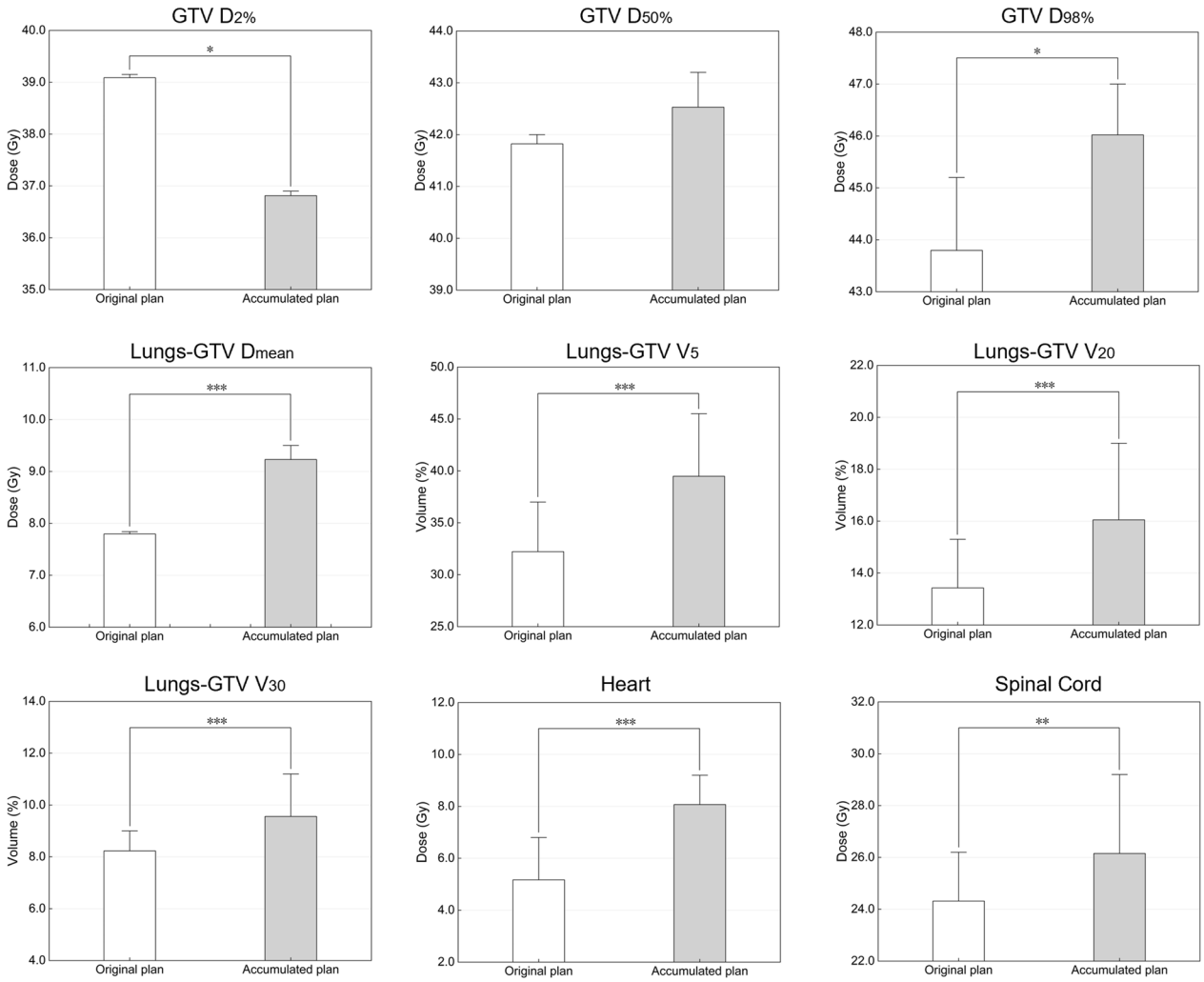

Fig. 6 Comparison of doses between the original plan and the accumulated plan. Asterisks indicated statistically significant differences, where * denoted $P < 0.05$, ** denoted $P < 0.01$, and *** denoted $P < 0.001$

to CRT alone. The dose evaluation parameters for all OARs, including lungs-GTV, heart, and spinal cord, demonstrated significant reductions, with differences achieving statistical significance ($P < 0.05$). Importantly, while the dose to lung tissues in the CRT plan approached the limit, it did not exceed it. For patients with large lung tumors, considering the decline in lung function and dose deviations due to uncontrollable respiratory motion, the adaptive LRT enhancement plan in conjunction with CRT effectively maintained lung toxicity within a safer range.

The results of the retrospective analysis on the off-target effects of the adaptive LRT enhancement plan regarding GTV and high-dose regions are presented in Fig. 8. In the sCT reconstructed from 19 free-breathing CBCT scan sequences, the relative displacement deviation of GTV and structure of $D_{95\%}$ from the tumor boundary did not exceed 5 mm, with inter-fraction deviations limited to 4 mm. This study excluded GTV delineation within 10 mm of the tumor boundary, thereby establishing an effective safety margin.

A defining feature of the LRT plan is the pronounced disparity between the peak and valley doses. Figure 9 presents the dose deviations measured at 20 TLD points in a heterogeneous anatomical model, comparing 60 independent measurements with the corresponding planned doses from the TPS. Of these measurements, 32 exhibited deviations of less than 2% (27 at the vertices and 5 in the valleys), while 5 exceeded 5% (4 at the vertices and 1 in the valleys), with the maximum deviation reaching 5.89%.

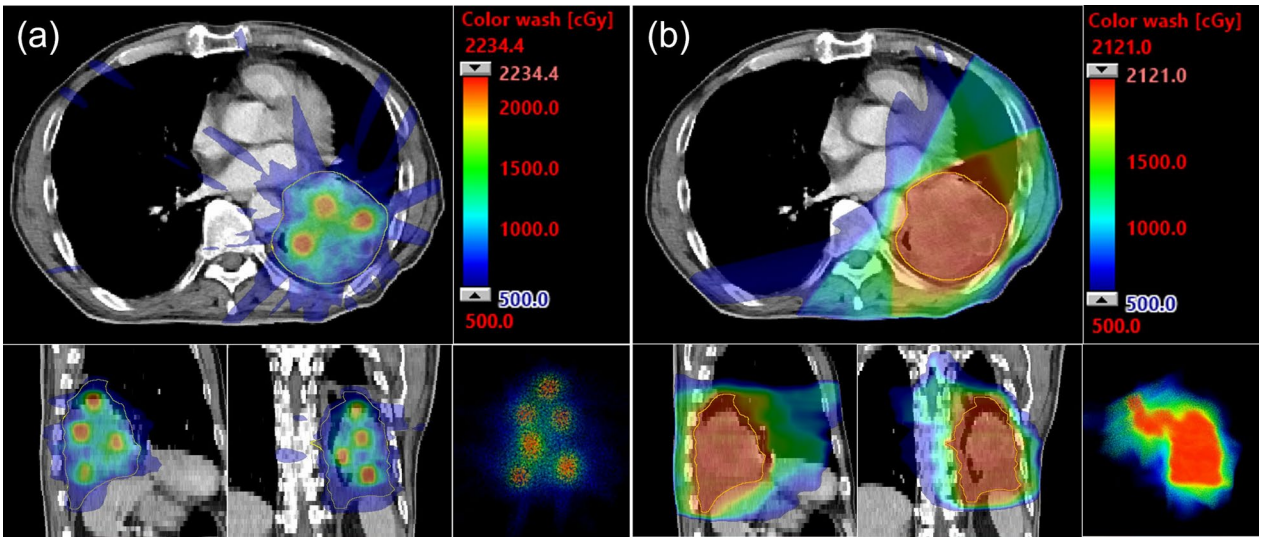

Fig. 7 Comparison of dose distributions between LRT and CRT for large lung tumors. Panel **a** presented the dose distribution of the LRT plan in axial, coronal, sagittal, and three-dimensional views; panel **b** presented the dose distribution of the CRT plan in the same planes and dimensions

Table 2 Dosimetric analysis of the actual doses received by OARs when utilizing LRT as a boost plan in comparison to CRT

Items	Dosimetry parameters	LRT	CRT	LRT + AD	CRT + AD	*P*-value
Lungs-GTV	Dmean (Gy)	0.97 ± 0.02	3.53 ± 0.34	10.36 ± 7.17	12.73 ± 1.85	0.010*
	V_5 (%)	1.01 ± 0.10	21.86 ± 5.73	43.10 ± 19.25	61.56 ± 5.14	< 0.001*
	V_{10} (%)	0.00 ± 0.00	11.18 ± 3.16	34.36 ± 16.92	48.90 ± 4.47	< 0.001*
	V_{15} (%)	0.00 ± 0.00	4.94 ± 0.93	22.25 ± 15.26	28.27 ± 5.54	0.001*
	V_{20} (%)	–	–	15.66 ± 11.52	21.82 ± 3.14	< 0.001*
	V_{30} (%)	–	–	9.62 ± 7.36	12.63 ± 1.29	< 0.001*
Heart	D_{mean} (Gy)	1.04 ± 0.64	2.84 ± 1.07	9.16 ± 6.04	10.34 ± 4.86	0.021*
Spinal cord	D_{max} (Gy)	5.54 ± 1.22	12.02 ± 1.98	32.44 ± 6.37	40.41 ± 5.11	0.007*

AD denoted the accumulated dose delivered in CRT mode for the initial 20 fractions, each prescribed at 2 Gy

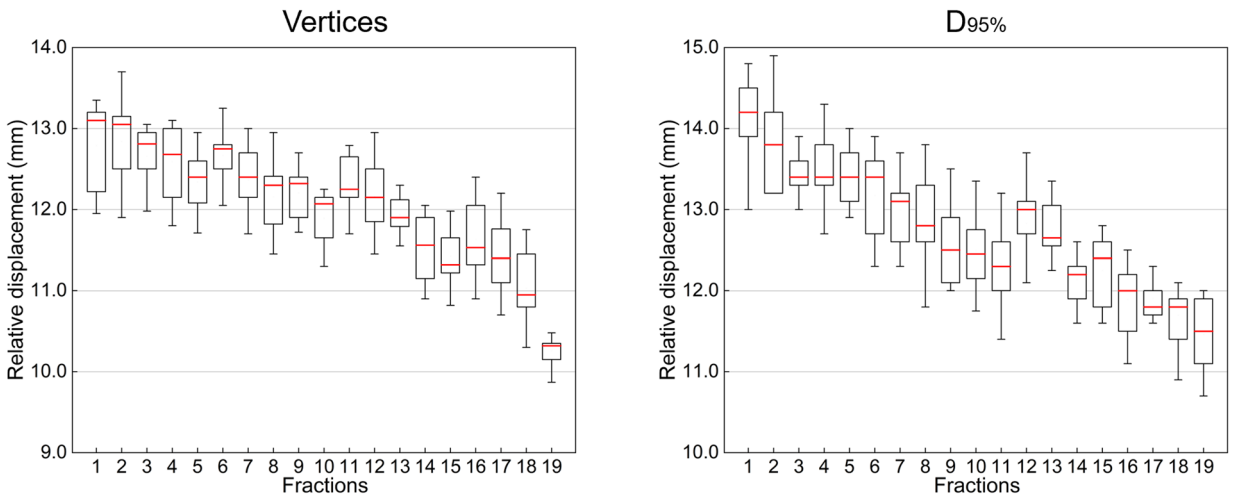

Fig. 8 Relative displacement of Vertices and structure of $D_{95\%}$ from the tumor boundary in 19 treatment fractions

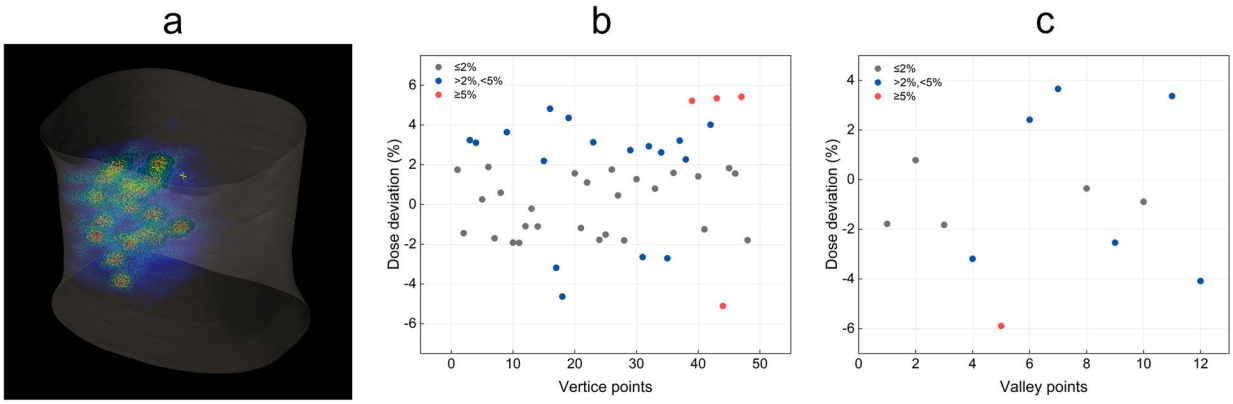

Fig. 9 Deviation between the measured doses and the corresponding planned doses from the TPS within a heterogeneous anatomical model. Panel **a** presented the dose distribution of the LRT plan in the heterogeneous anatomical model; panel **b** presented the dose deviations at vertice points of 48 measurements; panel **c** presented the dose deviations at valley points of 12 measurements

Discussion

Deep learning technologies have markedly advanced image reconstruction in medical imaging. Among these approaches, the Cycle-GAN and U-Net models are prominently utilized for medical image reconstruction [29, 30]. The Cycle-GAN model, operating within the framework of Generative Adversarial Networks, excels in generating high-quality images but often prioritizes global features over local details, particularly in complex anatomical structures. This limitation is critical in lung tumor imaging, where respiratory motion complicates accurate image production. Conversely, the U-Net model employs a multi-scale feature fusion strategy that effectively integrates features across scales, enhancing reconstruction accuracy [31, 32]. The U-Net++model, developed in this study, built on U-Net's dense feature fusion by introducing additional skip connections and improved feature processing, which significantly enhanced information flow and the retention of subtle structural details during high-resolution image reconstruction. Moreover, U-Net++effectively identified and mitigated artifacts induced by imaging parameters and respiratory motion during CBCT scans, thereby enhancing HU consistency. However, it is crucial to highlight that variations in the dataset and algorithm tuning necessitate comparisons among different algorithms. Such comparisons are an important area of inquiry, as they yield insights into the relative strengths and limitations of each approach.

Previous studies have established that high radiation dose in large lung tumor can result in severe side effects and mortality. Notably, steep dose gradients heighten the risk of toxicity to OARs, which are susceptible to anatomical changes. IGRT enhances the safety and efficacy of radiation treatment. However, Thomsen et al. found that geometric measurements from CBCT do not consistently correlate with changes in tumor or OARs dose [33]. Thus, accurate dose calculations, alongside geometric assessments, are crucial. Previous research indicates a dose calculation error of approximately 2–3% from CBCT, which does not meet clinical standards. In contrast, the accuracy error of dose calculations derived from sCT generated by the U-Net++model was maintained within 1.25%.

This study utilized acceptable dose calculation results from sCT to reveal significant discrepancies between the actual radiation doses received by the GTV and OARs in large lung tumor patients undergoing CRT, even with minimal tumor regression. Notably, the doses received by the lungs and heart were significantly excessive. This finding further corroborated the concern that geometric measurements assessed by radiation therapy technicians using CBCT may still have led to overdoses in OARs. By incorporating updated anatomical structures for organ segmentation between treatment fractions, we accurately assessed the radiation doses received by critical organs prior to implementing adaptive planning. This methodology not only provided essential references for subsequent boost treatments in large lung tumors with suboptimal CRT responses but also enhanced the accuracy of CRT, enabling timely identification and mitigation of potential overdose risks in critical organs.

The significance of ART lies in its ability to address dose deviations due to anatomical changes [34]. However, this capability is limited in large lung tumor, particularly when local control during CRT is inadequate. Additionally, the tolerance of normal tissues poses challenges in treating large, radioresistant tumors near critical structures, such as the spinal cord [35–37]. In contrast, LRT employs heterogeneous dose distributions,

challenging conventional CRT paradigms. The observed protection of normal tissues and improved tumor control with LRT are not adequately explained by traditional radiobiological concepts. Emerging evidence suggests that radiation effects in LRT may extend beyond cell death, incorporating non-targeted effects, such as the bystander effect, as well as stroma and immune response changes [38]. Therefore, LRT represents a valuable alternative for treating large lung tumor with inadequate local control under CRT.

Utilizing available clinical data and phase-specific physical guidelines, this study comprehensively explored the sCT based adaptive LRT boost plan, emphasizing dosimetric analysis. The typical LRT plan, combined with CRT, significantly reduced normal tissue toxicity compared to CRT alone. However, conventional DVH assessments were inadequate for evaluating the GTV. Instead, the EUD concept was frequently employed to predict tumor control efficacy [39, 40]. One form of EUD, proposed by Niemierko, was expressed as:

$$EUD_a = \left[\sum_i \left(v_i D_i^a\right)\right]^{\frac{1}{a}} \quad (1)$$

where v_i represented the volume fraction of the i th sub-volume receiving dose D_i, and a value was a scaling factor reflecting the characteristics of the tissue and its sensitivity to radiation. In CRT, the a value for tumors was typically a large negative number (e.g., -10). However, a review of existing clinical experiences with LRT suggested that the interpretation of the a value in this context remains ambiguous. Figure 10 illustrated a comparison of the DVH for both the LRT and CRT plans analyzed in this study, with EUD values corresponding to various a values also depicted. Notably, EUD_{-10} was measured at 5.59 Gy, indicating a high tumor control rate. In principle, an effective a value should be determined by comparing LRT to a series of uniform irradiations yielding equivalent tumor responses.

It is essential to acknowledge that patients with large lung tumors may experience dose deviations due to compromised pulmonary function and inadequate respiratory motion control, which increases the risk of target miss in the LRT plan. This study conducted a retrospective analysis of the positioning of the GTV and high-dose regions in the sCT across 19 random sequences during free breathing. The findings indicated that the ROIs and tumor boundaries consistently remained within a safe range. Considering the rapid dose drop characteristic of the vertices and valleys in LRT plan, the margin resulting from relative displacement further reduced the risk of target miss.

The dosimetry protocol is primarily dictated by the shape and size of the radiation beam and the resulting dose distribution. In LRT, high-dose regions typically exhibit a diameter of 1 cm or greater, facilitating dosimetric references from SBRT and the application of high-resolution diode arrays, electronic portal imaging devices, or radiographic films [41, 42]. This study proposed the implementation of TLD for direct dose measurements at the vertices and valleys of the adaptive LRT boost plan. Although TLD detectors are typically not used as routine instruments for radiation dose measurement in clinical quality control due to stringent

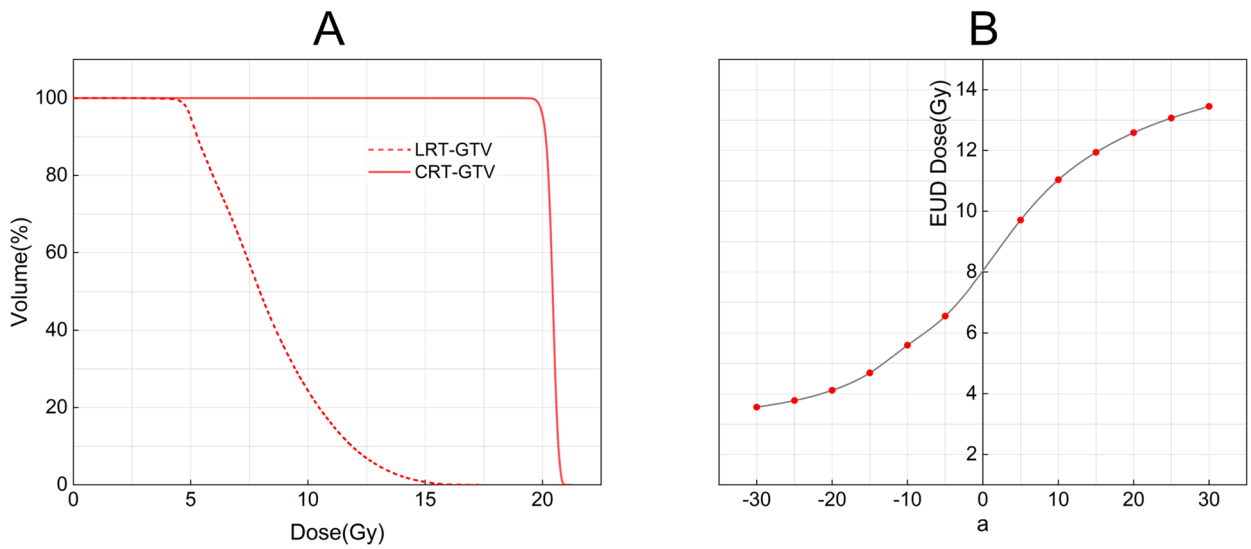

Fig. 10 Panel **A**: DVH of the GTV in LRT and CRT plan; panel **B**: The associated EUD is expressed as a function of the biological sensitivity scaling factor *a*

requirements for annealing and response measurement protocols, they consistently demonstrate measurement accuracy within 2 to 3% [43]. The results demonstrate good consistency between the actual delivered dose and the planned dose in sCT-based adaptive LRT boost plans for both vertices and valley regions. However, for high-dose plans targeting small volumes, additional refinement is required to improve patient validation between the TPS and actual accelerator delivery.

Conclusions

This study demonstrated that the U-Net++deep learning model enhanced CBCT image quality while improving dose calculation accuracy for clinical applications. Daily CBCT scans using Halcyon effectively monitored fractionated and accumulated dose distributions in patients with large lung tumors. The sCT-based adaptive LRT boost plan combined with CRT offered a viable treatment option for large lung tumors, particularly for patients with low tumor regression rates, and this study preliminarily validated its benefits in dose characteristics.

Abbreviations

CRT	Conventional radiotherapy
SBRT	Stereotactic body radiation therapy
OARs	Organs at risk
SFRT	Spatially fractionated radiotherapy
LRT	Lattice radiotherapy
DVH	Dose-volume histogram
IGRT	Image-guided radiotherapy
ART	Adaptive radiotherapy
CBCT	Cone-beam computed tomography
sCT	Synthetic CT
pCT	Planning CT
HU	Hounsfield unit
MAE	Mean absolute error
MSE	Mean squared error
SSIM	Structural similarity index measure
GTV	Gross tumor volume
IMRT	Intensity modulated radiation therapy
VMAT	Volumetric modulated arc therapy
ROIs	Regions of interest
DTA	Distance-to-agreement
DSC	Dice similarity coefficient
TPS	Treatment planning system
EUD	Equivalent uniform dose
TLD	Thermoluminescent dosimeter

Acknowledgements

Not applicable.

Author contributions

JY, RZ, and HZ conceived and designed the study. WS, WG, and YZ collected and assembled the data. HZ and XE constructed and optimized the model. ML, SZ and YF analyzed and interpreted the data. HZ wrote the manuscript.

Funding

This work was supported by the Shanghai Health Commission (Grant Number: 202340160) and the Science and Technology Development Project of Shanghai University of Traditional Chinese Medicine (Grant Number: 23KFL105).

Availability of data and materials

No datasets were generated or analysed during the current study.

Declarations

Ethics approval and consent to participate

Not applicable.

Consent for publication

Not applicable.

Competing interests

The authors declare no competing interests.

Author details

[1]Department of Radiotherapy, Shuguang Hospital Affiliated to Shanghai University of Traditional Chinese Medicine, Zhangheng Road, Pudong New Area, Shanghai 201203, China. [2]Department of Radiotherapy, Changzhou Cancer Hospital, Honghe Road, Xinbei Area, Changzhou 213032, China.

Received: 23 September 2024 Accepted: 4 December 2024
Published online: 22 January 2025

References

1. Siegel RL, Miller KD, Jemal A. Cancer statistics, 2019. CA Cancer J Clin. 2019;69(1):7–34.
2. Shiue K, Cerra-Franco A, Shapiro R, et al. Histology, tumor volume, and radiation dose predict outcomes in nsclc patients after stereotactic ablative radiotherapy. J Thorac Oncol. 2018;13(10):1549–59.
3. Lee P, Loo BW Jr, Biswas T, et al. Local control after stereotactic body radiation therapy for stage I non-small cell lung cancer. Int J Radiat Oncol Biol Phys. 2021;110(1):160–71.
4. Wang X, Bai H, Gao M, et al. Impact of radiation dose to the immune system on disease progression and survival for early-stage non-small cell lung cancer treated with stereotactic body radiation therapy. Radiother Oncol. 2023;186: 109804.
5. Das A, Giuliani M, Bezjak A. Radiotherapy for lung metastases: conventional to stereotactic body radiation therapy. Semin Radiat Oncol. 2023;33(2):172–80.
6. Yan W, Khan MK, Wu X, et al. Spatially fractionated radiation therapy: History, present and the future. Clin Transl Radiat Oncol. 2019;20:30–8.
7. Li H, Mayr NA, Griffin RJ, et al. Overview and recommendations for prospective multi-institutional spatially fractionated radiation therapy clinical trials. Int J Radiat Oncol Biol Phys. 2024;119(3):737–49.
8. Mayr NA, Mohiuddin M, Snider JW, et al. Practice patterns of spatially fractionated radiation therapy: a clinical practice survey. Adv Radiat Oncol. 2023;9(2):101308.
9. Blanco Suarez JM, Amendola BE, Perez N, Amendola M, Wu X. The use of lattice radiation therapy (LRT) in the treatment of bulky tumors: a case report of a large metastatic mixed mullerian ovarian tumor. Cureus. 2015;7(11):e389.
10. Zhang X, Penagaricano J, Yan Y, et al. Spatially fractionated radiotherapy (GRID) using helical tomotherapy. J Appl Clin Med Phys. 2016;17(1):396–407.
11. Zhang W, Lin Y, Wang F, Badkul R, Chen RC, Gao H. Lattice position optimization for LATTICE therapy. Med Phys. 2023;50(12):7359–67.
12. Amendola BE, Perez NC, Wu X, Blanco Suarez JM, Lu JJ, Amendola M. Improved outcome of treating locally advanced lung cancer with the use of lattice radiotherapy (LRT): a case report. Clin Transl Radiat Oncol. 2018;9:68–71.
13. Das IJ, Khan AU, Dogan SK, Longo M. Grid/lattice therapy: consideration of small field dosimetry. Br J Radiol. 2024;97(1158):1088–98.
14. Tekatli H, Haasbeek N, Dahele M, et al. Outcomes of hypofractionated high-dose radiotherapy in poor-risk patients with "ultracentral" non-small cell lung cancer. J Thorac Oncol. 2016;11(7):1081–9.

15. Lindberg K, Grozman V, Karlsson K, et al. The HILUS-trial-a prospective nordic multicenter phase 2 study of ultracentral lung tumors treated with stereotactic body radiotherapy. J Thorac Oncol. 2021;16(7):1200–10.
16. Rim CH, Kim Y, Kim CY, Yoon WS, Yang DS. Is stereotactic body radiotherapy for ultra-central lung tumor a feasible option? A systemic review and meta-analysis. Int J Radiat Biol. 2019;95(3):329–37.
17. Møller DS, Nielsen TB, Brink C, et al. Heterogeneous FDG-guided dose-escalation for locally advanced NSCLC (the NARLAL2 trial): design and early dosimetric results of a randomized, multi-centre phase-III study. Radiother Oncol. 2017;124(2):311–7. https://doi.org/10.1016/j.radonc.2017.06.022.
18. Sloth Møller D, Knap MM, Nyeng TB, et al. Difference in target definition using three different methods to include respiratory motion in radiotherapy of lung cancer. Acta Oncol. 2017;56(11):1604–9.
19. Underberg RW, Lagerwaard FJ, Slotman BJ, Cuijpers JP, Senan S. Use of maximum intensity projections (MIP) for target volume generation in 4DCT scans for lung cancer. Int J Radiat Oncol Biol Phys. 2005;63(1):253–60.
20. Zhou S, Meng Y, Sun X, Jin Z, Feng W, Yang H. The critical components for effective adaptive radiotherapy in patients with unresectable non-small-cell lung cancer: who, when and how. Future Oncol. 2022;18(31):3551–62.
21. Duan YH, Gu HL, Yang XH, et al. Evaluation of IGRT-induced imaging doses and secondary cancer risk for SBRT early lung cancer patients in silico study. Technol Cancer Res Treat. 2021;20:15330338211016472.
22. Ren XC, Liu YE, Li J, Lin Q. Progress in image-guided radiotherapy for the treatment of non-small cell lung cancer. World J Radiol. 2019;11(3):46–54.
23. Sonke JJ, Belderbos J. Adaptive radiotherapy for lung cancer. Semin Radiat Oncol. 2010;20(2):94–106.
24. Hattu D, Mannens J, Öllers M, van Loon J, De Ruysscher D, van Elmpt W. A traffic light protocol workflow for image-guided adaptive radiotherapy in lung cancer patients. Radiother Oncol. 2022;175:152–8.
25. Chen L, Liang X, Shen C, Jiang S, Wang J. Synthetic CT generation from CBCT images via deep learning. Med Phys. 2020;47(3):1115–25.
26. Chen L, Liang X, Shen C, Nguyen D, Jiang S, Wang J. Synthetic CT generation from CBCT images via unsupervised deep learning. Phys Med Biol. 2021. https://doi.org/10.1088/1361-6560/ac01b6.
27. Liu X, Yang R, Xiong T, et al. CBCT-to-CT Synthesis for cervical cancer adaptive radiotherapy via U-Net-based model hierarchically trained with hybrid dataset. Cancers (Basel). 2023;15(22):5479.
28. Wu X, Perez NC, Zheng Y, et al. The technical and clinical implementation of LATTICE radiation therapy (LRT). Radiat Res. 2020;194(6):737–46.
29. Deng L, Ji Y, Huang S, Yang X, Wang J. Synthetic CT generation from CBCT using double-chain-CycleGAN. Comput Biol Med. 2023;161: 106889.
30. Pang B, Si H, Liu M, et al. Comparison and evaluation of different deep learning models of synthetic CT generation from CBCT for nasopharynx cancer adaptive proton therapy. Med Phys. 2023;50(11):6920–30.
31. Chen Z, Chen S, Hu F. CTA-UNet: CNN-transformer architecture UNet for dental CBCT images segmentation. Phys Med Biol. 2023. https://doi.org/10.1088/1361-6560/acf026.
32. Landry G, Hansen D, Kamp F, et al. Comparing Unet training with three different datasets to correct CBCT images for prostate radiotherapy dose calculations. Phys Med Biol. 2019;64(3):035011.
33. Thomsen SN, Møller DS, Knap MM, Khalil AA, Shcytte T, Hoffmann L. Daily CBCT-based dose calculations for enhancing the safety of dose-escalation in lung cancer radiotherapy. Radiother Oncol. 2024;200:110506. https://doi.org/10.1016/j.radonc.2024.110506.
34. Barragán-Montero AM, Van Ooteghem G, Dumont D, Rivas ST, Sterpin E, Geets X. Dosimetrically triggered adaptive radiotherapy for head and neck cancer: considerations for the implementation of clinical protocols. J Appl Clin Med Phys. 2023;24(11): e14095.
35. Nestle U, Schimek-Jasch T, Kremp S, et al. Imaging-based target volume reduction in chemoradiotherapy for locally advanced non-small-cell lung cancer (PET-Plan): a multicentre, open-label, randomised, controlled trial. Lancet Oncol. 2020;21(4):581–92.
36. Schild SE, Hillman SL, Tan AD, et al. Long-term results of a trial of concurrent chemotherapy and escalating doses of radiation for unresectable non-small cell lung cancer: NCCTG N0028 (Alliance). J Thorac Oncol. 2017;12(4):697–703.
37. Pettersen MN, Aird E, Olsen DR. Quality assurance of dosimetry and the impact on sample size in randomized clinical trials. Radiother Oncol. 2008;86(2):195–9.
38. Wang R, Zhou T, Liu W, Zuo L. Molecular mechanism of bystander effects and related abscopal/cohort effects in cancer therapy. Oncotarget. 2018;9(26):18637–47.
39. Gay HA, Niemierko A. A free program for calculating EUD-based NTCP and TCP in external beam radiotherapy. Phys Med. 2007;23(3–4):115–25.
40. Wu Q, Mohan R, Niemierko A, Schmidt-Ullrich R. Optimization of intensity-modulated radiotherapy plans based on the equivalent uniform dose. Int J Radiat Oncol Biol Phys. 2002;52(1):224–35.
41. Amendola BE, Perez NC, Wu X, Amendola MA, Qureshi IZ. Safety and efficacy of lattice radiotherapy in voluminous non-small cell lung cancer. Cureus. 2019;11(3):4263.
42. Pollack A, Chinea FM, Bossart E, et al. Phase I trial of mri-guided prostate cancer lattice extreme ablative dose lead boost radiation therapy. Int J Radiat Oncol Biol Phys. 2020;108(1):328.
43. Low DA, Moran JM, Dempsey JF, Dong L, Oldham M. Dosimetry tools and techniques for IMRT. Med Phys. 2011;38(3):1313–38.

Publisher's Note